



ORIGINAL ARTICLE

Fabrication and characterizations of nanocomposite flexible films of ZnO and polyvinyl chloride/poly (N-vinyl carbazole) polymers for dielectric capacitors



A.A. Al-Muntaser^{a,*}, Essam Banoqitah^{b,c,*}, M.A. Morsi^{d,e}, Aysh Y. Madkhli^f,
J.A. Mohammed Abdulwahed^g, Reem Alwafi^h, Abdullah F. Al Naimⁱ,
Abdu Saeed^{h,j,*}

^a Department of Physics, Faculty of Education and Applied Sciences at Arhab, Sana'a University, Sana'a, Yemen

^b Nuclear Engineering Department, Faculty of Engineering, King Abdulaziz University, Jeddah 21589, Saudi Arabia

^c Center for Training & Radiation Prevention, King Abdulaziz University, Jeddah 21589, Saudi Arabia

^d Physics Department, Faculty of Science, Taibah University, Al-Ula, Medina, Saudi Arabia

^e Mathematical and Natural Sciences Department, Faculty of Engineering, Egyptian Russian University, Badr City, Cairo 11829, Egypt

^f Department of Physics, Faculty of Science, Jazan University, Jazan 45142, Saudi Arabia

^g Physics Department, Umm Al-Qura University College in Qunfudah-Female, Saudi Arabia

^h Department of Physics, Faculty of Science, King Abdulaziz University, Jeddah 21589, Saudi Arabia

ⁱ Department of Physics, College of Science, King Faisal University, P.O. Box 400, Al-Ahsa 31982, Saudi Arabia

^j Department of Physics, Thamar University, Thamar 87246, Yemen

Received 22 April 2023; accepted 14 July 2023

Available online 20 July 2023

KEYWORDS

PVC;
PVK;
ZnO nanoparticles;
Nanocomposites;
Energy storage

Abstract Polymer-based energy storage has recently attracted the attention of researchers. Herein, via the sol-gel method, we prepared zinc oxide nanoparticles (ZnO NPs), as nanofiller up to 5 wt% filling levels, and a host polymeric blend matrix of polyvinyl chloride (PVC) and poly (N-vinyl carbazole) (PVK) were taken to synthesize nanocomposite films via the solution casting. The ratio of PVC: PVK was 90:10 wt%. The X-ray diffraction (XRD) results indicated that the prepared nanocomposite films' crystallinity decreased as ZnO NPs content increased; it decreased from 54.23 to 22.14 %. The scanning electron microscope (SEM) micrographs revealed good miscibility of the prepared PVC/PVK blend and the homogeneous distribution of ZnO NPs within the host blend matrix. The thermal stability of the prepared nanocomposites was studied through the

* Corresponding authors at: Department of Physics, Faculty of Education and Applied Sciences at Arhab, Sana'a University, Sana'a, Yemen (A. Al-Muntaser); Nuclear Engineering Department, Faculty of Engineering, King Abdulaziz University, Jeddah 21589, Saudi Arabia (E. Banoqitah); Department of Physics, Faculty of Science, King Abdulaziz University, Jeddah 21589, Saudi Arabia (A. Saeed).

E-mail addresses: almuntser2015@gmail.com, ali.almuntasser@su.edu.ye (A.A. Al-Muntaser), ebanoqitah@kau.edu.sa (E. Banoqitah), Abdusaeed@tu.ed.ye, Abdusaeed79@hotmail.com (A. Saeed).

<https://doi.org/10.1016/j.arabjc.2023.105171>

1878-5352 © 2023 The Author(s). Published by Elsevier B.V. on behalf of King Saud University.

This is an open access article under the CC BY license (<http://creativecommons.org/licenses/by/4.0/>).

TGA technique, and the thermal activation energy was calculated using the Coats-Redfern method. In the optical results, the optical absorption spectra revealed that the energy gap for the allowed direct transition reduced under adding ZnO NPs; it reduced from 3.61 eV for the pure PVC/PVK blend to 2.96 eV for the nanocomposite film with ZnO nanofiller content of 5 wt%. AC conductivity experiments revealed that the electrical/dielectric properties of the nanocomposite films get enhanced by increasing the ZnO NPs content. Following the incorporation of the ZnO NPs, the AC electrical conductivity (σ_{ac}), dc electrical conductivity (σ_{dc}), dielectric constant (ϵ'), and dielectric loss (ϵ'') values of PVC/PVK/ZnO nanocomposite films get improved; the σ_{dc} values increased from 6.46×10^{-16} S/cm for the blend PVC/PVK matrix to 3.63×10^{-13} S/cm for nanocomposites with ZnO NPs content of 5 wt%. Additionally, both ϵ' and ϵ'' values increased while increasing the ZnO NPs content. These findings could suggest that the prepared PVC/PVK/ZnO nanocomposite films could be a promise for the applications of dielectric energy storage polymer-based capacitors.

© 2023 The Author(s). Published by Elsevier B.V. on behalf of King Saud University. This is an open access article under the CC BY license (<http://creativecommons.org/licenses/by/4.0/>).

1. Introduction

Polymer-based energy storage has become a popular topic among researchers lately (Michael and Prabaharan, 2004; Menazea et al., 2020; Tarabiah et al., 2022; Morsi et al., 2022; Al-Muntaser et al., 2023; Al-Muntaser et al., 2023; El Gohary et al., 2023; Saeed et al., 2023), as they offer a better alternative choice for electrical power systems and modern electronic applications. They have unique advantages, such as working at high voltage, low cost/simple processing, and fast charge/discharge (Liu et al., 2016). Therefore, the fabricating and processing of new polymers for polymer-based energy storage will contribute to the solution energy problem.

Polyvinyl chloride (PVC) is a valuable industrial polymer with numerous applications (Nikam and Deshpande, 2018). As a result of its low cost, high recovery rate, and excellent electrical and corrosion resistance (Miliute-Plepiene et al., 2021), it is commonly used in the industry. PVC is commonly mixed with several polymers (Zhang et al., 2020; Ranjan et al., 2021; Yang et al., 2009). The organic semiconducting polymer poly(N-vinyl carbazole) (PVK) contains molecules consisting of repeating groups of atoms (Das et al., 2017). It is the most vastly recognized polymeric photoconductor (Ahlatcioğlu Özerol, 2019); here, its carbazole group allows it to be used in optical and electric devices (Lai et al., 2005; Choudhury et al., 2004). PVK has high thermal conductivity, low optical absorption, and a high refractive index in visible and infrared ranges (Alghunaim, 2018). Its photophysical characteristics make it an ideal polymer for electro-optically active material in xerography (Moisan et al., 1991) and light-emitting diodes (Das et al., 2016; Wang et al., 2000). Recently, it has been utilized as a matrix for assessing low molecular weight compounds. In the field of energy storage, it was used to design lithium-ion batteries (Menazea et al., 2020) and rechargeable lithium batteries based on hybrid polymer electrolytes (Michael and Prabaharan, 2004).

PVK is a carbazole derivative of PVC, where the chlorine atom in PVC $[(C_2H_3Cl)_n]$ is replaced by the carbazole group ($C_{12}H_9N$) to form PVK $[(C_{14}H_{11}N)_n]$ (Michael and Prabaharan, 2004). Therefore, they can be blended to produce composites with excellent compatibility. In most cases, mixing two or more polymers is cheaper and faster than discovering novel polymer chemistry to advance novel polymer composite with unique properties (El Miri et al., 2016). Many studies (Alghunaim, 2018; Krylov et al., 2016; Berestennikov and Aleshin, 2017) were concerned with analyzing the physical and chemical properties of the doped PVC/PVK mix with nanoparticles and carbon materials.

Nanoparticles (NPs) in the polymer can create nanocomposites exhibiting enhanced physical properties (Al-Muntaser et al., 2022b, 2022c; Bet-Moushoul et al., 2016). As a result of their blend of parts, nanocomposites can exhibit properties with new behaviors (Pleša et al., 2016). A new substitute for conventionally filled poly-

mers is introduced via nanocomposite of polymer and NPs (El-Kader et al., 2013). The development of novel and cutting-edge functions within the polymer matrix is made possible by including both organic polymers and NPs through these NPs. Alghunaim studied (Alghunaim, 2018) the impact of silicon carbide (SiC) NPs on the structural and optical properties, besides the electrical characteristics of the PVC/PVK blend, was studied. When the filler percentages boosted from 0.00 to 0.08 wt%, they discovered that SiC decreased the values of the energy gap from 3.82 to 0.73 eV. Besides, the PVC/PVK composite exhibited improved AC electrical conductivity as a result of the increased SiC content (Alghunaim, 2018). The impact of lead(II) oxide (PbO) NPs on the mechanical and thermal characteristics of a composite PVC/PMMA material has been studied by Gamal and Elsayed (El-Gamal and Elsayed, 2020), where the PVC/PMMA composite's thermal stability and thermal expansion were improved.

Zinc oxide (ZnO) nanoparticles (NPs) possess remarkable electrochemical and physicochemical properties, particularly their optical characteristics and chemical stability (Tarabiah et al., 2022). It is a semiconductor with a wide bandgap and unique properties such as low toxicity and high optical/thermal stability (Wang et al., 2021). As a result, it has been used in many applications, such as a gas sensor (Onkar et al., 2020), cleaner for drinking water/wastewater (Dimapilis et al., 2018), solar cells, luminescence (Willander et al., 2010), UV-blocking (Sasani Ghamsari et al., 2017), and energy storage devices (Fahimi and Moradlou, 2020). ZnO NPs have been incorporated with different polymers for different purposes, such as producing high luminescence emitters (Abdullah et al., 2003), polymer thermal stabilization (Cho et al., 2004), optoelectronics devices (Willander et al., 2011), enhancing tribological properties (Sudeepan et al., 2014), and antibacterial applications (Kubacka et al., 2009).

After looking through the articles and extensive studies on the impact of ZnO in polymers, to the best of our knowledge, there is no research on the effects of ZnO NPs on the structural, optical, and electrical/dielectric properties of this blend (PVC/PVK). This study focuses on creating PVC/PVK/ZnO nanocomposite films using the solution casting process and analyzing their structural, optical, and electrical characteristics. We employed X-ray diffraction (XRD) and Fourier-transform infrared spectroscopy (FTIR), scanning electron microscopy (SEM), and thermogravimetric analysis (TGA) techniques to investigate the structural, morphological, and thermal characteristics of prepared nanocomposites. Transmission electron microscopy (TEM) was utilized to explore the ZnO NPs' morphology prepared via the sol-gel method. UV/visible spectroscopy (UV/Vis) was used to determine the optical characteristics. Besides, we investigated the electrical/dielectric properties of nanocomposites made of PVK, PVC, and ZnO NPs to assess their promising applications in energy storage devices.

2. Experimental

2.1. Chemicals

In this study, the PVC and PVK were from Sigma Aldrich (Sigma–Aldrich, Germany). Ethanol (CH_2COOH) and Zinc acetate dihydrate [$\text{Zn}(\text{O}_2\text{CCH}_3)_2(\text{H}_2\text{O})_2$] with 99% of purity (Hm bG Chemical, Germany), sodium hydroxide (NaOH) pellets reagent grade with purity $\geq 98\%$ (Sigma Aldrich, Germany), were used to prepare the ZnO NPs. The PVK and PVC were dissolved in tetrahydrofuran (THF) from Al-Gamhoreih company (Al-Gamhoreih company, Mansoura, Egypt). The chemicals were utilized as received without any further purifications.

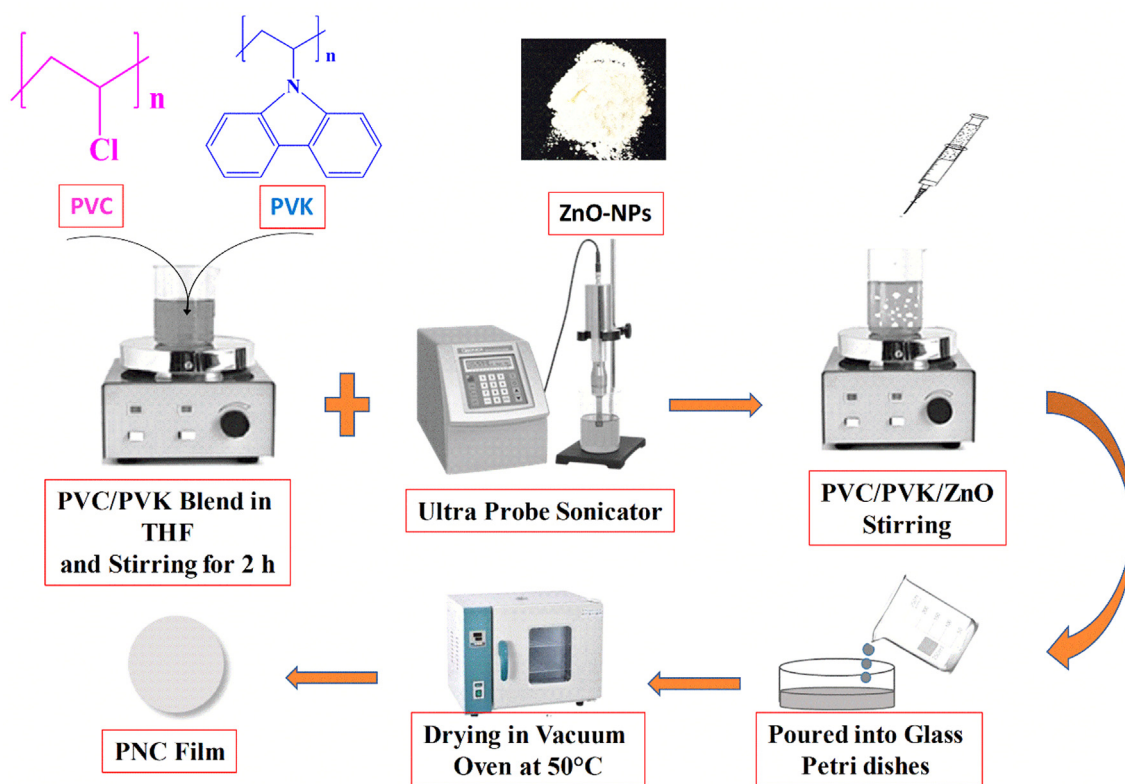
2.2. Nanocomposites' preparation

First, we prepared ZnO NPs via the sol–gel method reported in the published work (Al-Muntaser et al., 2022a, 2022c). Then, in 40 mL of THF, 1.26 g of PVC and 0.14 g of PVK (90:10) were dissolved with stirring at 40 °C for about 6 h (h) to form a solution. The prepared ZnO NPs were suspended in THF and then exposed to a high-power probe sonicator, specifically the model Q500 Sonicator (20 kHz, 500 W) from (QSONICA, USA), for a duration of 9 min. Afterward, ZnO NPs were added to the PVC/PVK blend solution at 1, 3, and 5 wt%. The resulting solution was incorporated into a Petri dish. Nanocomposites, comprised of both pure blend and PVC/PVK/ZnO nanocomposite at ZnO NPs contents of 1, 3, and 5 wt%, were generated after three days of progressive solvent

evaporation in the oven at a temperature of 50 °C. Peeled off the Petri plate, the resulting films ranged from 0.13 to 0.21 mm. Finally, the PVC/PVK/ZnO NPs nanocomposite films were used for characterizations and investigations. Scheme 1 illustrates the preparation steps of the PVC/PVK/ZnO NPs films.

2.3. Characterizations

We recorded the XRD patterns of prepared films (PVC/PVK/ZnO NPs) using x-ray diffractometer model X'Pert PRO (Malvern PANalytical, USA) with a Ni filter and Cu $K\alpha$ radiation of $\lambda = 15.406 \text{ \AA}$. FTIR analysis using model Nicolet iS10 (Thermo Scientific, USA) was utilized to identify the functional groups in PVC/PVK/ZnO NPs. The nanocomposite films' surfaces were investigated through SEM, model JEOL-JSM-7600f (JEOL, USA); their thermal features were analyzed using thermogravimetric analysis (TGA), model STA 409CD (NETZSCH, Germany) with 10 °C/min heating rate in a nitrogen environment. TEM model JEOL 1200 EX (JEOL, Japan) was employed to explore the size and form of ZnO NPs. By means of the UV/Vis spectrophotometer V-630 model (JASCO, Japan), the UV/Vis spectra of the prepared nanocomposite samples were investigated at room temperature. Concept Turnkey dielectric, conductivity, and impedance spectrometers with temperature control model Concept 40 (Novocontrol Technologies GmbH & Co. KG, Germany) was utilized to analyze the prepared nanocomposite films' electric/dialectical properties over the frequency range of 0.1 Hz to 20 MHz.



Scheme 1 The preparation steps of the PVC/PVK/ZnO nanocomposite films.

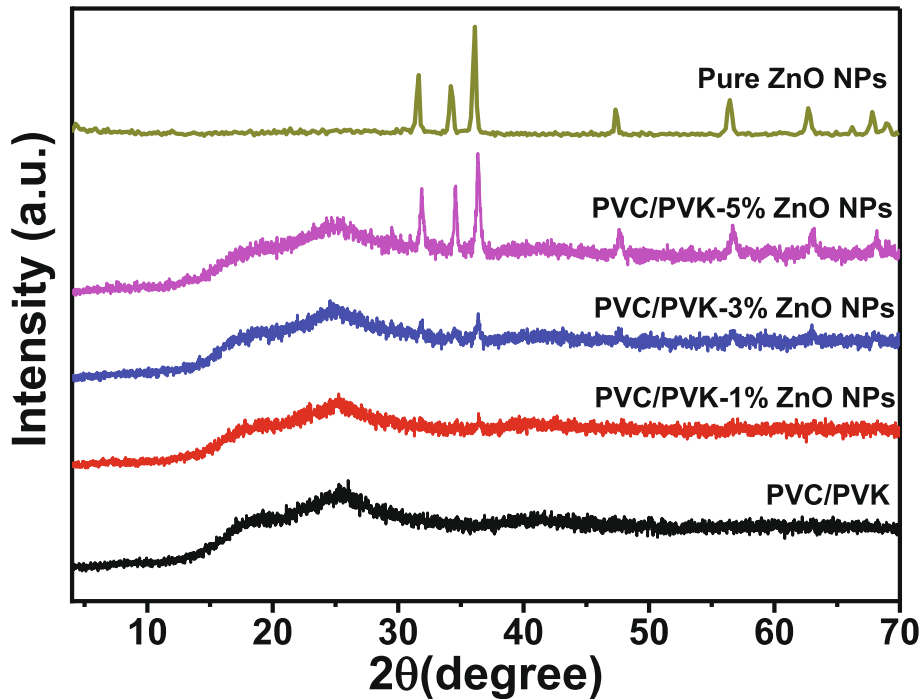


Fig. 1 XRD patterns of the prepared PVC/PVK/ZnO nanocomposite films at ZnO NPs content of 1, 3, and 5 wt%, besides the pure PVC/PVK and pure ZnO NPs.

3. Results and discussion

3.1. XRD and TEM

Fig. 1 shows the XRD patterns of prepared PVC/PVK blend, PVC/PVK/ZnO nanocomposite films (1, 3, and 5 wt%), and pure ZnO nanopowder. The XRD pattern of pure ZnO NPs shows reflection peaks at $2\theta \approx 31.61^\circ$ (100), 34.20° (002), 36.11° (101), 47.45° (012), 56.54° (110), 62.68° (013), 66.14° (200), 67.80° (112), and 68.84° (201). Based on JCPDS Card No. 01-089-0510 and the published works (Soliman et al., 2020; Hezma et al., 2019; Jiménez-Rosado et al., 2022), these diffraction peaks were indexed to the atomic planes of (100), (002), (101), (012), (110), (013), (200), (112), and (201), depicting the hexagonal Wurtzite crystal structure with cell lattice parameters of $a = b = 3.2493 \text{ \AA}$ and $c = 5.2057 \text{ \AA}$. Using Scherrer's equation (Abdelrazek et al., 2018), the mean crystallite size was 18.07 nm. The XRD pattern of pure PVC/PVK blend exhibits two broad peaks at $2\theta \approx 17.97$ and 25.63° explaining the amorphous nature of the polymer blend. Al-Muntaser et al. (Al-Muntaser et al., 2020) and Taha (Taha, 2017) reported that the amorphous PVC polymer shows two humps at $2\theta = 17$ and 25.50° . Abd El-kader et al. (Abd El-kader et al., 2015) and Menazea et al. (Menazea et al., 2018) indicated that the PVK polymer presented amorphous characteristics by showing two halos at $2\theta = 7.90^\circ$ and 23.10° . Therefore, the two broad peaks in the XRD scan of the amorphous PVC/PVK blend were attributed to the PVC polymer with content (90 wt%) within the blend structure and the disappearance of characterized halos of PVK results from the complexation between PVC/PVK chains. The reduction in the intensity and the increase of the two main peaks of PVC/PVK with the ZnO

NPs addition imply the rise of the degree of amorphously of the filled samples because of the intermolecular interactions between these NPs and the host blend matrix that raise the amorphous regions' content and soften the segmental motion of blend chains. From the XRD pattern of the nanocomposite sample (1 wt%), the diffraction peaks attributed to ZnO phases are not observed. However, at ZnO NPs contents ≥ 3 wt%, diffraction peaks are observed at $2\theta = 31.68, 34.54, 36.55, 47.71, 56.63, 63.12, 68.14,$ and 69.1° that can be attributed to ZnO NPs, and that their intensities increase largely at 5 wt% content. This result demonstrates the presence of ZnO NPs within the prepared nanocomposites.

The broadening in the XRD patterns could be understood via Hodge et al. (Hodge et al., 1996), who found a relationship between peak intensity and crystallinity level, where the peak intensity of the XRD pattern might reduce as the amorphousness of the material increase as a result of the dopant addition. Therefore, the crystallinity (X_c) was determined by equation (1), reported by Hermans and Weidinger (Hermans and Weidinger, 1949):

$$X_c = \left(\frac{A_c}{A_T} \right) \times 100\% \quad (1)$$

where A_T is the total area of peaks (the area of the amorphous and crystalline diffracted peaks), and A_c is the area of the amorphous haloes. The obtained crystallinity values are summarized in Table 1. As indicated in this table, the crystallinity dropped from 54.23% for the pure PVC/PVK blend to approximately 22.14% for the PVC/PVK samples doped with 5 wt% ZnO NPs. The increase in the amorphous phase of the polymer matrix in the PVC/PVK/ZnO nanocomposite films could suggest improvements in the conductivity properties, as well as considerable mobility, where it was reported

Sample	Pure PVC/PVK	PVC/PVK-1% ZnO NPs	PVC/PVK-3% ZnO NPs	PVC/PVK-5% ZnO NPs
Crystallinity (%)	54.23	41.34	36.73	22.14

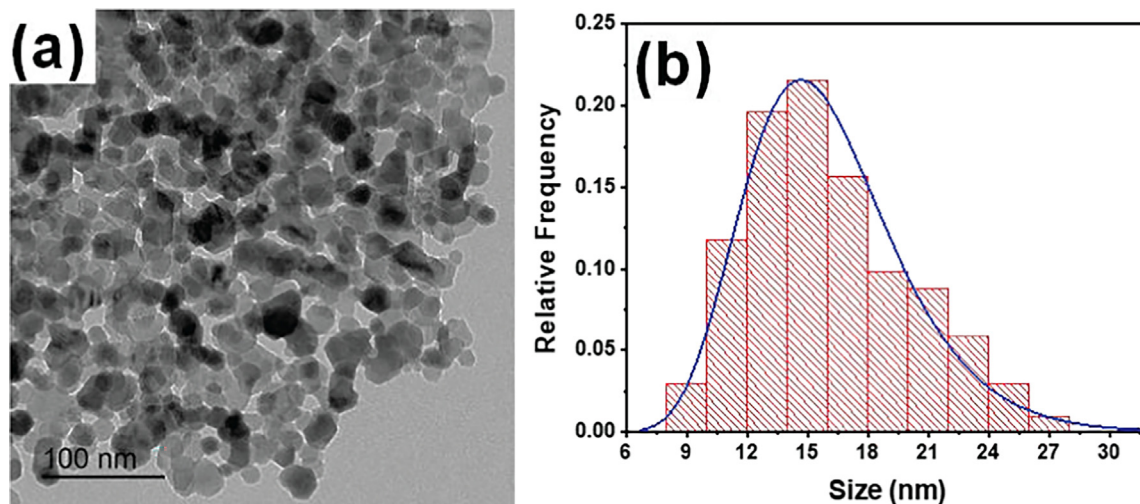


Fig. 2 (a) TEM photomicrograph of the ZnO NPs prepared via sol-gel (b) histogram distribution of the ZnO NPs' particle size.

(Croce et al., 1998) that the nanofiller could enhance ionic conductivity, in which fast ion transport is a characteristic of the amorphous phase.

Fig. 2 shows the TEM results; here, Fig. 2a displays the TEM photomicrograph for the ZnO NPs prepared via the sol-gel method. The ZnO NPs appear to have an almost near-hexagonal shape; this result agrees with those reported shapes of ZnO NPs prepared using the sol-gel method (Chelouche et al., 2014; Zhang et al., 2010). The prepared NPs show aggregation behavior that could result from their suspension in deionized water before dropping in the carbon-coated copper grids (200 mesh) for TEM imaging. The particle sizes for ZnO NPs were in the range of 8–28 nm; Fig. 2b displays a histogram distribution for the particle sizes. The distribution was fitted using the lognormal distribution function; lognormal distribution is derived from a normal distribution using logarithmic mathematics, suggesting the prepared particles' sizes distribution is nearly homogeneous. The ZnO NPs derived by sol-gel showed particle size with a mean value of 15 nm.

3.2. SEM analysis

SEM technique is utilized to verify the distribution and dispersion of ZnO NPs within the PVC/PVK matrix and investigate the surface of the prepared films. Fig. 3 illustrates the SEM images for the two virgin polymers (PVC and PVK), pure PVC/PVK blend, and blend/ZnO nanocomposite samples. From Fig. 3a–b, the images of PVC and PVK polymers have homogeneous and smooth surfaces without cracks and pores, reflecting their amorphous structure as indicated in the XRD data. The same images were reported by Taha et al. (2019) and Menazea et al. (2018). From Fig. 3c, the surface of pure PVC/PVK also seems smooth; this could indicate a good mis-

ibility/coherence between the blend's components. With the addition of ZnO NPs, the surface of filled samples becomes rougher due to the existence of small white granules. The near disappearance of the ZnO from the surface of the nanocomposite film (1 wt%) is because of the good dispersion of the nanofiller and its presence in small filling levels. These morphological variations could imply a good dispersion of added NPs within the PVC/PVK structure and their uniform distribution on the surface, where the interbreeding between the PVC/PVK matrix and ZnO NPs is apparent.

3.3. FTIR study

FTIR investigation is an essential tool for establishing the interactions between PVC/PVK blend and ZnO NPs. FTIR spectra of both the PVC/PVK blend and the PVC/PVK/ZnO nanocomposite films at ZnO NPs content of 1, 3, and 5 wt% show the most characteristic infrared vibrational modes (Fig. 4). The major vibrational bands for PVC/PVK have been assigned. The bands, which appear in the spectral range of 3250–2750 cm^{-1} , are due to the C–H bonds' symmetric and asymmetric stretching vibration modes in the methyl and methylene groups of both PVC and PVK polymers (Malimabe et al., 2020; Kaur et al., 2022; Tinh et al., 2012). The bands between 1485 and 1398 cm^{-1} could be referred to as the symmetrical bending vibration modes of C–H bonds, whereas the bands in the range 1136–1049 cm^{-1} could result from the stretching of C–C bonds (Malimabe et al., 2020). The bands between 990 and 888 cm^{-1} are ascribed to C–H bond bending modes (Kaur et al., 2022). The bands in the range 790–700 cm^{-1} belong to out-of-plane bending vibration modes of the aromatic –C–H group in PVK, besides the less intensity band located at 1602 cm^{-1} , which is attributed to the C=C stretching vibration of the vinylidene group (PVK)

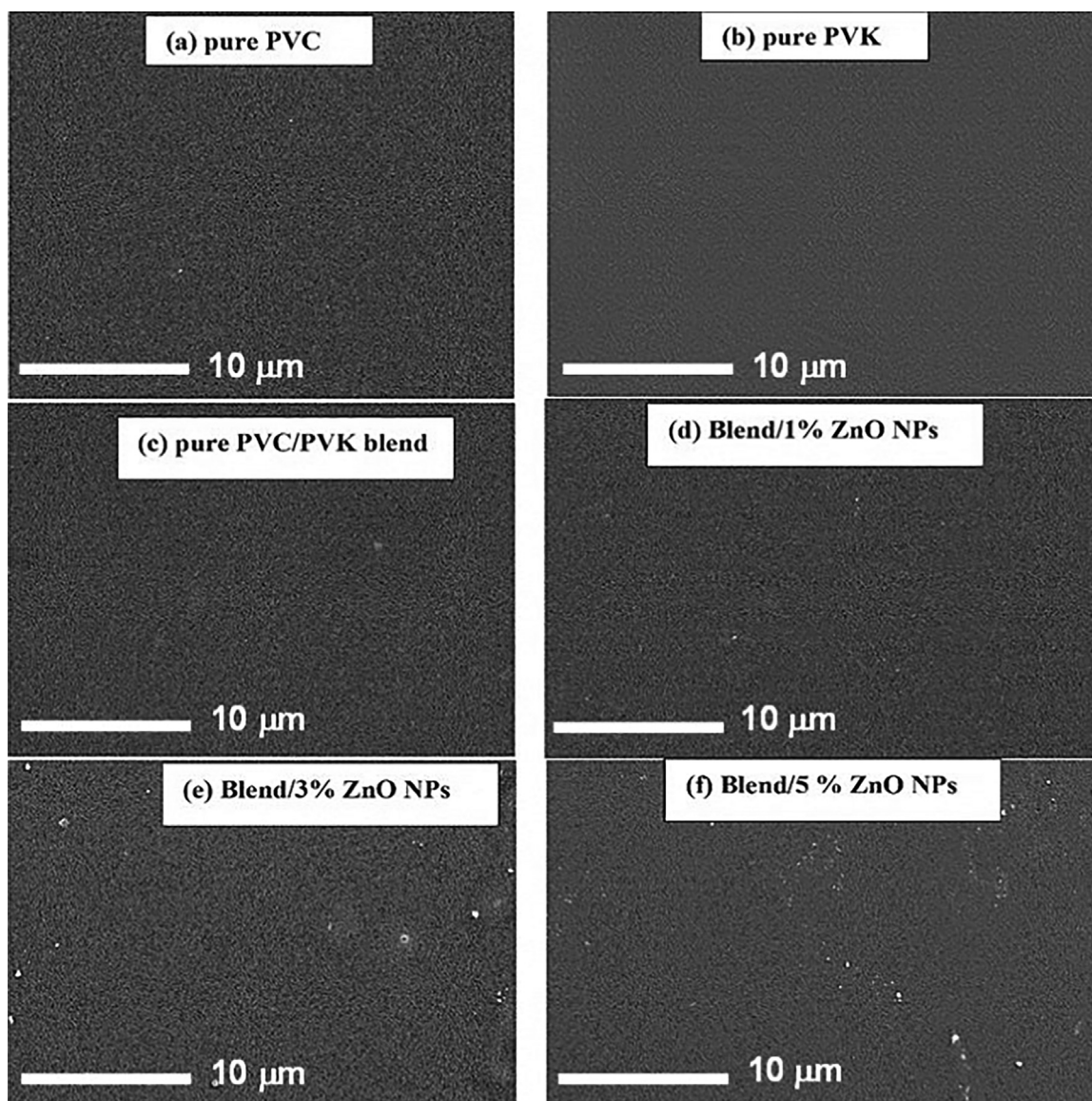


Fig. 3 SEM micrographs of pure PVC, pure PVK, pure Pure PVC/PVK blend, and PVC/PVK/ZnO NPs nanocomposite samples.

([Thin et al., 2012](#)). Before comparing the intensities of the peak of the samples' spectra, normalization, which is a spectroscopic correction to avoid if there is any difference in the concentrations of the samples ([O'Rourke et al., 2019](#)), was applied for all the samples' spectra. The spectra showed that the intensities of all the characteristic bands in prepared PVC/PVK/ZnO nanocomposite films weaken as ZnO NPs content increases. The decrease in the intensities of FTIR spectra peaks with the increase in the content of ZnO NPs could be explained through the decrease in the polymer blend ratio.

3.4. TGA

The TGA analysis of pure PVC, pure PVK, pure PVC/PVK blend, and PVC/PVK/ZnO nanocomposite films are indicated in [Fig. 5](#). A three-stage decomposition steps can be observed in the TGA of pure PVC polymer ([Fig. 5a](#)) ([Taha, 2017](#); [Jakić et al., 2013](#); [Nair et al., 2007](#)), where the first stage (180–

250 °C) of a weight loss (3%) attributes to the moisture evaporation and THF dispersal. The second (265–360 °C) and final (410–525 °C) stages correspond to weight loss values of 45% and 73%. The second stage was referred to as the HCl-elimination “dehydrochlorination,” leaving behind longer polyene chains. The thermal decomposition of the carbon chain and polyene sequences exists in the third thermal stage producing volatile aliphatic/aromatic compounds through the intramolecular cyclization of the conjugated sequences. The residual weight (9%) at temperature > 525 °C corresponds to the remaining char.

Pure PVK exhibits a two-step decomposition pattern ([Fig. 5a](#)) that begins with a small, steady loss at ~330 °C because of the decomposition of the PVK chains ([Menazea et al., 2018](#); [Cui et al., 2011](#); [Santos et al., 2012](#)). The fast second decomposition step reaches a 90% weight loss at 330 °C, corresponding to the cleavage backbone of the polymer as the PVK structure suffers from the random chain scission of

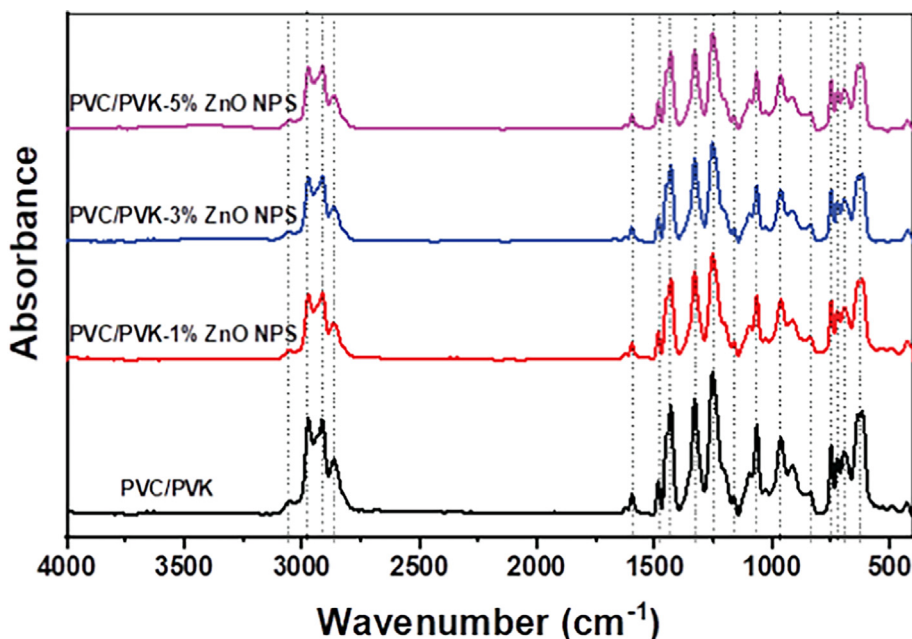


Fig. 4 FT-IR spectra of the prepared PVC/PVK/ZnO nanocomposite films at ZnO NPs content of 1, 3, and 5 wt%, besides the pure PVC/PVK.

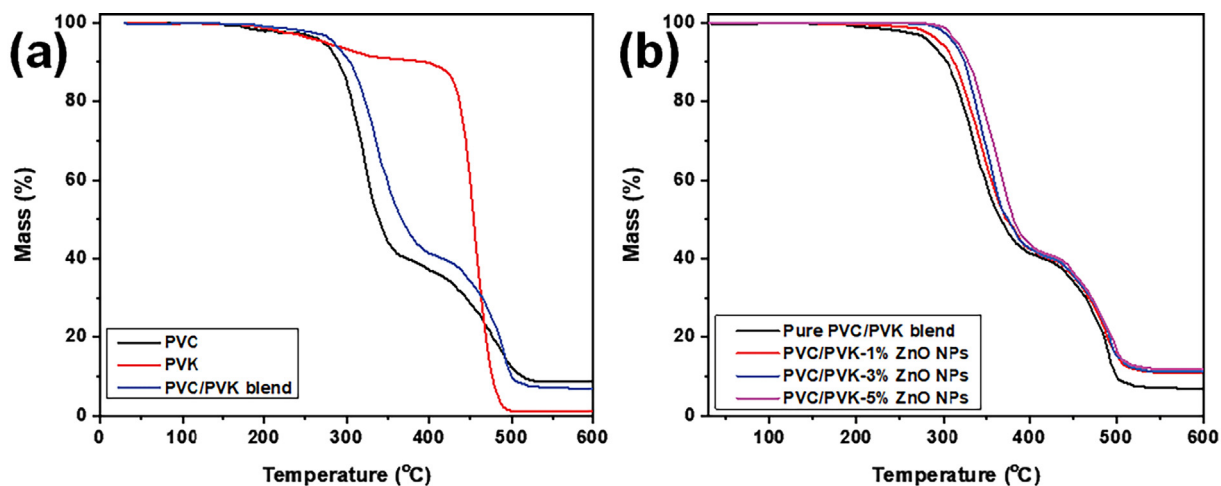


Fig. 5 TGA of (a) pure PVC, pure PVK, and pure PVC/PVK blend, and (b) PVC/PVK/ZnO nanocomposite films.

C—H, N—H, and C=C groups during the thermal degradation.

The degradation of pure PVC/PVK blend shows a similar pattern as pure PVC polymer due to the high content of PVC within the prepared blend matrix and exhibits three-step decomposition. It is clear that the TGA curve of the blend possesses higher stability than that of pure PVC, which could be a sign of the PVK thermal stabilizing effect on PVC due to the interactions between the functional groups of the blend's components delay the dehydrochlorination of PVC within the blend.

For the various compositions of PVC/PVK/ ZnO nanocomposite samples, the trend of TGA curves is similar

to pure blend by showing three thermal degradation stages. These curves shift toward high-temperature values and show a lower weight loss (%) at ~ 510 °C compared to the pure blend, which is assigned to the existence of thermally stable ZnO NPs that boost heat dissipation within the nanocomposite films. Table 2 reports the extracted mass loss values at temperatures (300, 400, and 500 °C) values and residual weight at 600 °C. From this table and Fig. 5b, the increased thermal stability of the filled samples can be attributed to the good dispersion of ZnO NPs (Hezma et al., 2019; Taha, 2017; Menazea et al., 2018; Abutalib and Rajeh, 2020), as it prevents the flux of decomposition product and, therefore, hinder the degradation process. The PVC/PVK chains around ZnO NPs may

Table 2 The values of weight loss at various temperatures, residual weight, and E_a for pure PVC/PVK blend and (b) PVC/PVK/ZnO nanocomposite films.

Samples	Weight loss (%)			Residual weight (%)	E_a (kJ/mol)
	300 °C	400 °C	500 °C		
Pure PVC/PVK	9.18	59.13	90.21	7.03	1.18
PVC/PVK-1% ZnO NPs	5.93	58.23	85.52	10.58	1.06
PVC/PVK-3% ZnO NPs	2.68	57.14	84.79	11.31	0.93
PVC/PVK-5% ZnO NPs	1.24	56.06	83.35	12.17	0.867

decompose more slowly, which assists in moving the thermal degradation temperatures to higher values. Thus, the PVC/PVK/ZnO nanocomposite samples have good thermal stability, which is needed for their processing applications, such as polymer batteries.

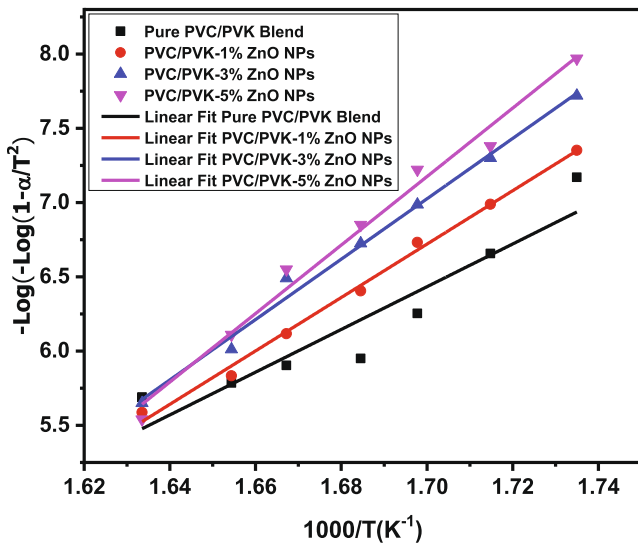
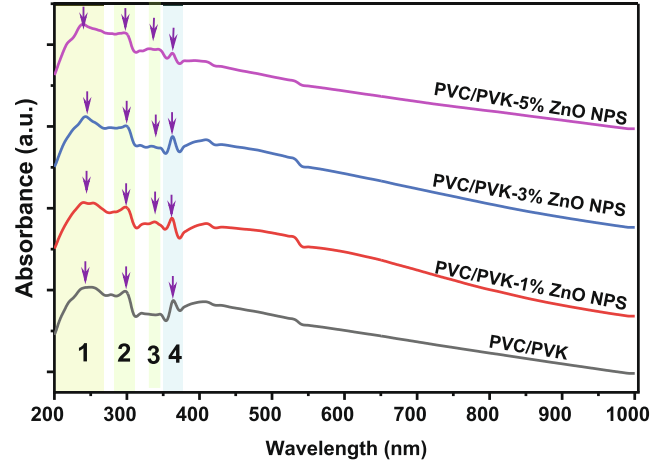
The thermal kinetics of the PVC/PVK/ZnO nanocomposite films can be obtained from the TGA curves at the main degradation step by using the Coats-Redfern method (Coats and Redfern, 1964) as follow:

$$\log \left[\frac{-\log(1-\alpha)}{T^2} \right] = \log \frac{R}{E_a} \left[1 - \frac{2RT}{E_a} \right] - \frac{1}{2.303} \frac{E_a}{RT} \quad (3)$$

where E_a is the activation energy, R is the real gas constant, and α is the fractional weight loss at that particular temperature = $\frac{\text{Initial weight } (w_i) - \text{Weight at given temperature } (w_t)}{w_i - \text{Final weight } (w_f)}$. The relation between $-\log[-\log(1-\alpha)/T^2]$ and $1000/T$ is shown in Fig. 6, and the E_a values are calculated from the slopes and listed in Table 2. The increase in the filling level of ZnO NPs resulted in a reduction in E_a , depicting the easy segmental motion of the polymeric chains of the PVC/PVK blend.

3.5. Optical measurement

Fig. 7 displays the UV/Vis spectra of the PVC/PVK blend, besides PVC/PVK/ZnO nanocomposite films at ZnO NPs con-

**Fig. 6** Plots of Coats-Redfern relation for pure PVC/PVK blend and PVC/PVK/ZnO nanocomposite films.**Fig. 7** The UV/vis spectra of the pure PVC/PVK blend and PVC/PVK/ZnO nanocomposite films at ZnO NPs content of 1, 3, and 5 wt%.

tent of 1, 3, and 5 wt% in the spectra range between 200 and 1000 nm. The tested samples' UV/Vis spectra showed four absorption peaks; the broad peak centered at around 242 nm corresponded to $\pi \rightarrow \pi^*$ electronic transition (Menazea et al., 2020). The second peak is a small but sharp absorption centered at 298 nm, and the third peak, which is also sharp, centered at around 362 nm; these two peaks were attributed to $n \rightarrow \pi^*$ electronic transition; these two peaks, i.e., the second and third belong to the phenyl ring exists in each repeat unit in the structure of the polymers (Sonone et al., 2014). The third peak showed a weak absorbance peak at 337 nm; this peak was not observed in the pure PVC/PVK blend. This peak could be attributed to the surface plasmon resonance (SPR) of the ZnO NPs (Hezma et al., 2019; Abutalib and Rajeh, 2020; Choudhary, 2018), depicting NPs within the PVC/PVK structure. It is evident that the intensity of the second and fourth absorption peaks in the prepared nanocomposites faint with rising ZnO NPs concentrations; this result could be referred to as the interaction impacts of the ZnO NPs as fillers in the PVC/PVK polymers matrix. This result corresponds to and confirms the results obtained by FTIR.

It is essential to investigate and determine the average optical energy gap (E_g) values to comprehend the optical characteristics and parameters of the nanocomposite. The nature of the film and the distribution and arrangement of molecules within the polymeric chain all affect the E_g values. The energy gap of the PVC/PVK blend and PVC/PVK/ZnO nanocompos-

ite films was studied using the absorption band at the UV area. Where the E_g was estimated via the Tauc equation:

$$(\alpha h\nu)^{1/n} = A(h\nu - E_g) \quad (2)$$

where α and ν are the absorption coefficient and photon frequency, respectively; A is a constant; h is the Planck constant. Where n obeys the quantum selection rules; here, $n = 1/2$ or 2 for allowed direct or indirect electronic transitions, respectively; $n = 3/2$ for direct forbidden transition (Morsi et al., 2022; Almashhori et al., 2020; Kim, 2018; Rehman et al., 2023).

Fig. 8 exhibits the Tauc plot of the PVC/PVK blend and PVC/PVK/ZnO nanocomposite films at ZnO NPs contents of 1, 3, and 5 wt% in both direct (Fig. 8a) and indirect (Fig. 8b) transitions. The value of E_g for each sample was assessed through the extrapolation of the plot of $(\alpha h\nu)^2$ linear regions against $h\nu$ (direct transition) and $(\alpha h\nu)^{1/2}$ against $h\nu$ (indirect transition). Both extracted optical band gap energy, direct (E_{gd}) and indirect (E_{gi}), are listed in Table 3. The values of E_{gd} decreased from 3.61 eV for pure PVC/PVK polymers to 2.96 eV for the PVC/PVK/ZnO nanocomposite film at the highest ZnO NPs content, i.e., 5 wt%; also, the E_{gi} values decreased from 0.56 to 0.13 eV.

3.6. Electrical study

3.6.1. AC conductivity

Measuring the electrical conductivity of the materials is a significant step in determining the transport mechanisms in polymeric nanocomposites. Fig. 9 shows the AC conductivity at room temperature for pure PVC/PVK and PVC/PVK/ZnO nanocomposite films at ZnO NPs content of 1, 3, and 5 wt% versus logarithms of frequency (f). It can be seen that the pure PVC/PVK showed AC conductivity, which increased linearly as the frequency increased. This behavior can be understood by that the electrical field can induce charge carriers that contribute to and enhance the electrical conductivity (Saeed et al., 2021; Alharbi et al., 2018). The PVC/PVK/ZnO nanocompos-

ite film at ZnO NPs content of 1 wt% showed nearly behavior and values similar to the pure PVC/PVK, suggesting no effect for ZnO NPs at the lowest content, i.e., 1%. However, The PVC/PVK/ZnO nanocomposite films at ZnO NPs content of 3 and 5 wt% exhibited two behaviors, the first at lower frequencies, where the AC electrical conductivity appeared constant while increasing the frequency. The AC electrical conductivity increased linearly at higher frequencies in the second behavior.

The AC electrical conductivity behaviors of the PVC/PVK/ZnO nanocomposite films at ZnO NPs content of 3 and 5 wt% could occur due to the non-equilibrium trap charges in the polymeric materials, the AC conductivity in the lower frequency region is nearly not frequency independent, where the conductivity decreases as a result of increased charge gathering at the electrode contact. Conductivity results in the high-frequency range rising exponentially as a function of frequency, which is compatible with charge carrier hopping. Hopping and Koop's law can be used to explain how conductivity increases with frequency (Koops, 1951). According to Koop's theory, conductivity is regulated and caused by grain boundaries with poor conductivity at lower frequencies. The hopping theory, which states that the electrical conductivity increases by improving the charge carrier's hopping between the polymer materials of PVC/PVK and the ZnO NPs, also could explain why conductivity increases with frequency (Elashmawi and Al-Muntaser, 2021). Conducting grains are the reason for the conductivity dispersion seen at higher frequencies. Furthermore, the ZnO NPs integration into the PVC/PVK composite improves the charge conduction mechanism significantly more quickly, as evidenced by the higher σ values of the PVC/PVK doped films compared with the blend polymers. This improvement could be referred to as the decrease in the crystallinity (see the XRD results), which improves disorders, and subsequently enhances the mobility of charge carriers, particularly ions transport (Croce et al., 1998). Since the nanocomposite polymer electrolytes are a type of flexible solid-state or quasi-solid-state ion-dipolar complexes, and these nanocomposites allow ion transportation to

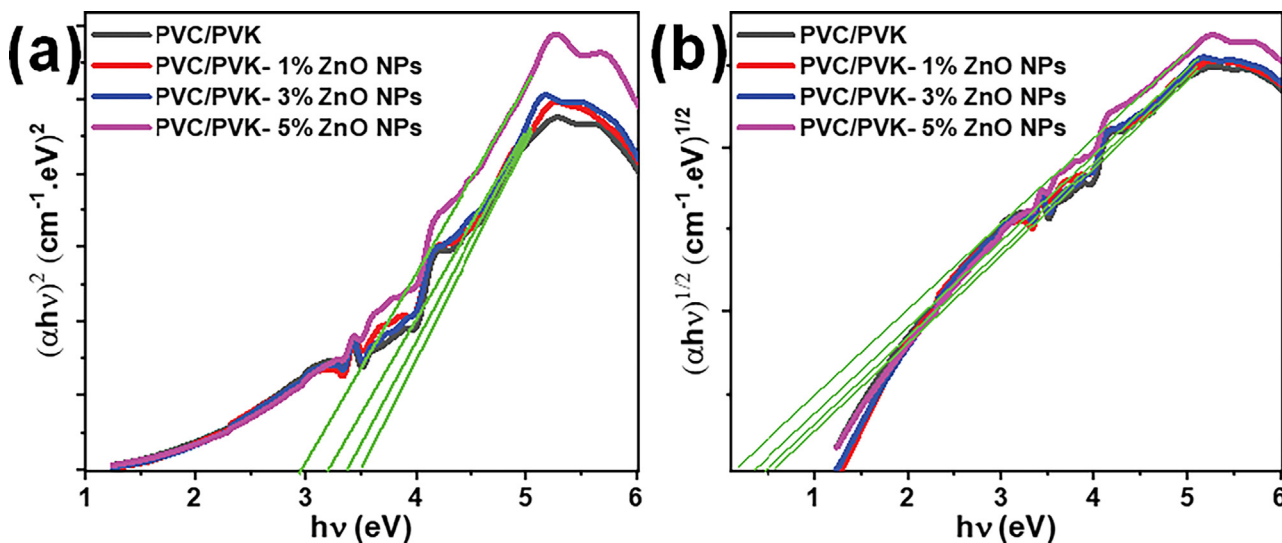


Fig. 8 The optical band gap energy of the PVC/PVK blend and PVC/PVK/ZnO nanocomposite films at ZnO NPs content of 1, 3, and 5 wt% for both (a) direct and (b) indirect transitions.

Table 3 The results of the energy gap, i.e., E_{gi} and E_{gd} of the pure PVC/PVK and PVC/PVK/ZnO nanocomposite films at ZnO NPs content of 1, 3, and 5 wt%.

Sample	Pure PVC/PVK	PVC/PVK-1% ZnO NPs	PVC/PVK-3% ZnO NPs	PVC/PVK-5% ZnO NPs
E_{gd} (eV)	3.61	3.48	3.38	2.96
E_{gi} (eV)	0.56	0.41	0.39	0.13

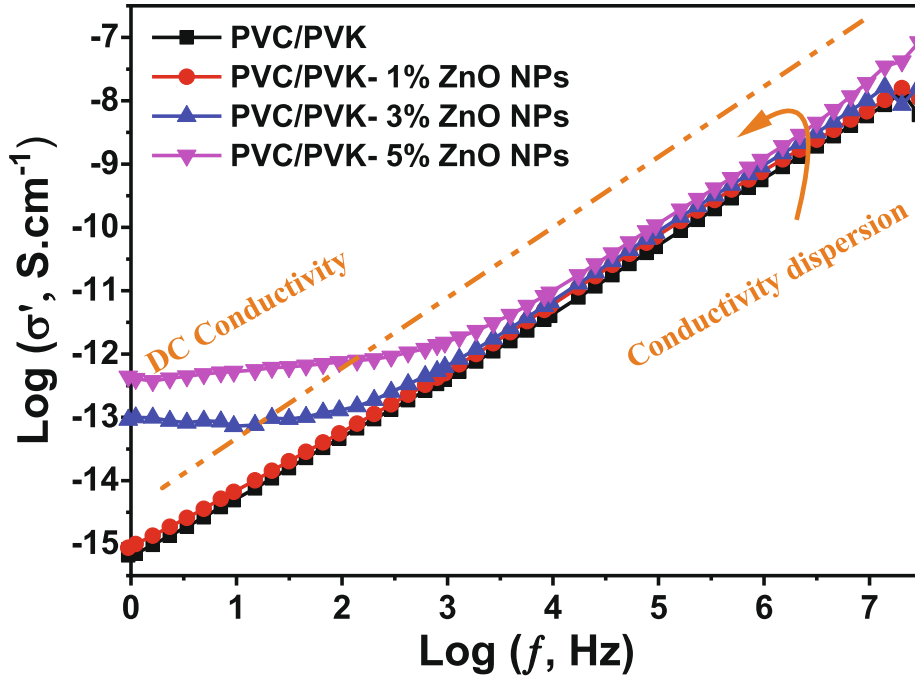


Fig. 9 AC electrical conductivity of the prepared PVC/PVK blend and PVC/PVK/ZnO nanocomposite films at ZnO NPs content of 1, 3, and 5 wt%.

happen alongside the movement of polymer chain segments, particularly within the amorphous polymer phase (Dhatarwal et al., 2018).

Also, the dc electrical conductivity of pure PVC/PVK and PVC/PVK/ZnO nanocomposite films at ZnO NPs content of 1, 3, and 5 wt% was measured; their obtained values are listed in Table 4. Pure PVC/PVK was $6.46 \times 10^{-16} \Omega^{-1} \cdot \text{cm}^{-1}$ as the lowest dc electrical conductivity in all tested samples; dc electrical conductivity increased while increasing the ZnO nanofillers to reach $3.63 \times 10^{-13} \Omega^{-1} \cdot \text{cm}^{-1}$ as the highest value for the PVC/PVK/ZnO nanocomposite film at ZnO NPs content of 3 wt%.

3.6.2. Dielectric study

We investigated the dielectric properties to estimate whether the prepared PVC/PVK/ZnO nanocomposite films can be used

in the polymer-based capacitors' design. For the investigation of dielectric properties, both dielectric constant (ϵ') and dielectric loss (ϵ'') are involved in to estimate. The dielectric constant measures the ability of the material to store energy, while the dielectric loss measures the energy dissipation in the material (Saeed et al., 2021, 2022). Fig. 10 displays the measured ϵ' and ϵ'' of the prepared PVC/PVK blend and PVC/PVK/ZnO nanocomposite films at ZnO NPs content of 1, 3, and 5 wt%; both of them were measured in the frequency range starting from 0.1 Hz up to 20 MHz. The prepared PVC/PVK/ZnO nanocomposite films showed improvements in values of ϵ' and ϵ'' compared with the prepared PVC/PVK blend polymer. This result could be due to the ZnO NPs, which were reported to have high orientation polarizability (Kurniawan et al., 2017), causing an enhancement in the dielectric properties in the nanocomposites. Also, it could result from the accumula-

Table 4 The values of σ_{dc} electrical conductivity for the prepared pure PVC/PVK and PVC/PVK/ZnO nanocomposite films at ZnO NPs content of 1, 3, and 5 wt%.

Sample	Pure PVC/PVK	PVC/PVK-1% ZnO NPs	PVC/PVK-3% ZnO NPs	PVC/PVK-5% ZnO NPs
σ_{dc} ($\Omega^{-1} \text{cm}^{-1}$)	6.46×10^{-16}	8.71×10^{-16}	4.37×10^{-14}	3.63×10^{-13}

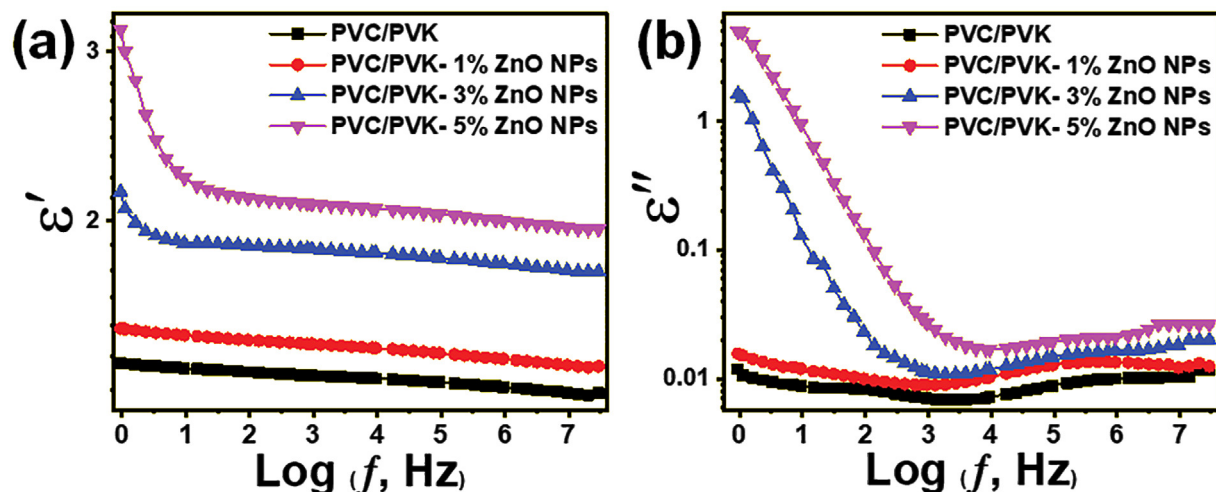


Fig. 10 Dielectric results of the prepared PVC/PVK blend and PVC/PVK/ZnO nanocomposite films at ZnO NPs content of 1, 3, and 5 wt% (a) dielectric constant and (b) dielectric constant.

tion of the charges in the grain boundaries of the ZnO NPs, creating space charge polarization in the nanocomposites. The relation between the ϵ' and the logarithm of the frequency for the prepared nanocomposite is shown in Fig. 10a. At the same time, Fig. 10b exhibits the relation between ϵ'' and the logarithm of the frequency. The values of ϵ' and ϵ'' rise rapidly toward lower frequency because dipoles in the nanocomposite film could follow and track the orientation of the changeable applied electric field at the lower frequency. However, at high frequencies, the applied electric field changes very fast; as a result, the charge carriers couldn't follow the change in the applied field, causing lowers values of both dielectric constants and dielectric losses (Ramesh and Liew, 2013). In the conclusion of dielectric properties, the ϵ' and ϵ'' values increased while increasing the ZnO NPs content. This impact could be due to the free charge carriers, which build up at the electrode-sample interfaces (Alghunaim, 2018), suggesting the prepared PVC/PVK/ZnO nanocomposite films could be a promise for the

applications of dielectric energy storage polymer-based capacitors.

3.6.3. Electric modulus

The electric modulus (M^*), a complex quantity, was utilized to study the phenomenon of conductivity relaxation and electrode effect (Yu et al., 2000). It is also useful to recognize and distinguish between electrode polarization and bulk effects. The formulas (3)–(5) are applied to determine the M' , M'' , and M^* :

$$M^* = M' - iM'' = \frac{1}{\epsilon^*} = \frac{\epsilon' + i\epsilon''}{(\epsilon')^2 + (\epsilon'')^2} \quad (3)$$

$$M' = \frac{\epsilon'}{\epsilon'^2 + \epsilon''^2} \quad (4)$$

$$M'' = \frac{\epsilon''}{\epsilon'^2 + \epsilon''^2} \quad (5)$$

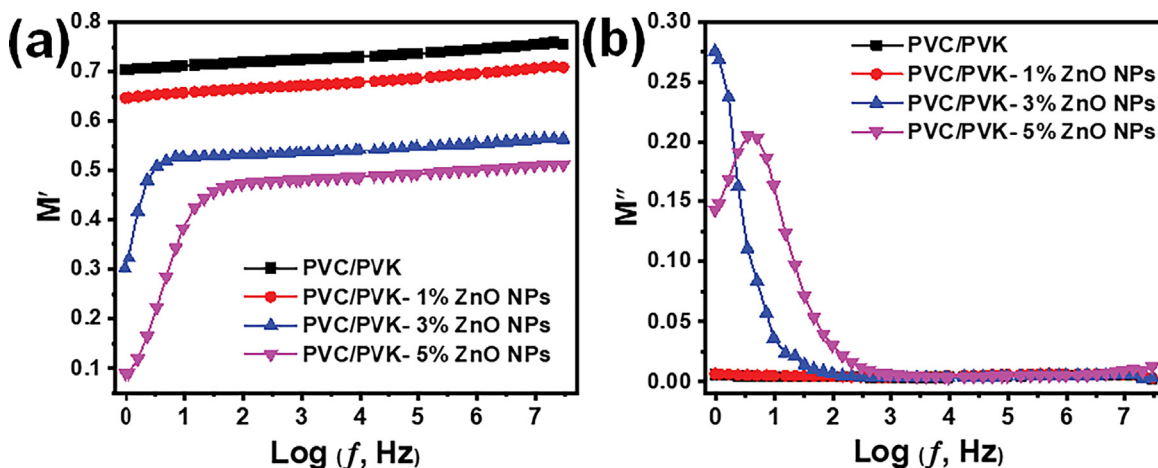


Fig. 11 Electric modulus of the prepared PVC/PVK blend and PVC/PVK/ZnO nanocomposite films at ZnO NPs content of 1, 3, and 5 wt% (a) real part (b) imaginary part.

here, M' and M'' are the electric modulus' real and imaginary parts, respectively. For the prepared PVC/PVK blend and PVC/PVK/ZnO nanocomposite films at ZnO NPs content of 1, 3, and 5 wt%, the values of M' and M'' versus the logarithm of the frequency were plotted in Fig. 11a and b, respectively. As shown in Fig. 11a, M' for the PVC/PVK blend and PVC/PVK/ZnO nanocomposite film at ZnO NPs content of 1 wt% showed nearly constant values with gradually tiny increases while increasing the frequency. This result could suggest an isotropic and homogeneous material without the effects of Maxwell-Wagner polarization (Misra et al., 2020). While for the prepared nanocomposite at ZnO NPs contents of 3 and 5 wt%, M' showed a step-like transition where it showed lower values at lower frequencies and then increased to reach nearly constant values at high frequencies. This phenomenon could happen (Langar et al., 2017) because of the short-range mobility of charge carriers resulting from ZnO NPs and the ease of conducting ions migration in the polymer matrix. The step-like existence from low to high in the M' values for the prepared nanocomposite at ZnO NPs contents of 3 and 5 wt% means the presence of a relaxation process will be seen in the M'' values.

It can be observed that the values of M'' demonstrated, as expected, the nature of the relaxation processes with its broad, well-defined peaks at ZnO NPs content of 5 wt%. The obtained sample is most probably ionic conductors, according to the M'' relaxation peak. In contrast, the pure PVC/PVK blend and nanocomposite at ZnO NPs content of 1 wt% (lowest dropped) showed no peak maximum, suggesting that the ZnO-NPs contribute to the relaxation process.

4. Conclusion

The solution casting process was utilized to prepare PVC/PVK/ZnO nanocomposite films at ZnO NP contents of 1.0, 3.0, and 5.0 wt%; the ZnO NPs were prepared via the sol-gel method. XRD results show that adding ZnO NPs decreases the crystallinity degree for the polymer matrix in the nanocomposite. The prepared ZnO NPs, as a filler in the nanocomposites, have a spherical shape with a mean particle size of 15 nm. The SEM micrographs illustrated that ZnO NPs were well dispersed within the PVC/PVK blend. From the TGA curves, the prepared nanocomposites showed better thermal stability, depicting that the existence of ZnO NPs inhibited/delayed the breakdown of the PVC/PVK backbone. The optical results revealed that the direct and indirect optical band gaps for the prepared PVC/PVK/ZnO nanocomposite films were decreased with the addition of ZnO as a result of the creation of a charge transfer complex between the PVC/PVK polymer as a matrix and the nanohybrid atoms. AC conductivity experiments revealed that the ϵ' and ϵ'' values of the PVC/PVK/ZnO nanocomposite films increased with increasing the ZnO NPs contents; besides, the σ_{dc} values of the PVC/PVK/ZnO nanocomposite films get improved nearly 2000 folds compared with the pure PVC/PVK blend polymers where the σ_{dc} values of PVC/PVK/ZnO NPs films improved from 6.46×10^{-16} S/cm for the blend of PVC/PVK to 3.63×10^{-13} S/cm for PVC/PVK/ZnO nanocomposite film at ZnO NPs content 5.0 wt% ZnO NPs. The findings of this study indicate that the prepared PVC/PVK/ZnO nanocomposite films could be a promise for the applications of flexible capacitors for dielectric energy storage polymer-based.

Declaration of Competing Interest

The authors declare that they have no known competing financial interests or personal relationships that could have appeared to influence the work reported in this paper.

Acknowledgment

This work was funded by Institutional Fund Projects under no. (IFPIP: 1616-135-1443). The authors, therefore, gratefully acknowledge the technical and financial support provided by the Ministry of Education and King Abdulaziz University, DSR, Jeddah, Saudi Arabia.

References

- Abd El-kader, F., Hakeem, N., Elashmawi, I., Menazea, A., 2015. Synthesis and characterization of PVK/AgNPs nanocomposites prepared by laser ablation. *Spectrochim. Acta A Mol. Biomol. Spectrosc.* 138, 331–339.
- Abdelrazek, E.M., Abdelghany, A.M., Badr, S.I., Morsi, M.A., 2018. Structural, optical, morphological and thermal properties of PEO/PVP blend containing different concentrations of biosynthesized Au nanoparticles. *J. Mater. Res. Technol.* 7 (4), 419–431.
- Abdullah, M., Lenggoro, I.W., Okuyama, K., Shi, F.G., 2003. In situ synthesis of polymer nanocomposite electrolytes emitting a high luminescence with a tunable wavelength. *J. Phys. Chem. B* 107 (9), 1957–1961.
- Abutalib, M., Rajeh, A., 2020. Influence of ZnO/Ag nanoparticles doping on the structural, thermal, optical and electrical properties of PAM/PEO composite. *Phys. B Condens. Matter* 578, 411796.
- Ahlatcioğlu Özerol, E., 2019. Electro-optical properties of poly(N-vinyl carbazole) nanoclay composites. *Polym. Bull.* 76 (10), 5301–5311.
- Alghunaim, N.S., 2018. Structural, thermal, dielectric spectroscopic and AC impedance properties of SiC nanoparticles doped PVK/PVC blend. *Results Phys.* 9, 1136–1140.
- Alharbi, S.R., Alhassan, M., Jalled, O., Wageh, S., Saeed, A., 2018. Structural characterizations and electrical conduction mechanism of $\text{CaBi}_2\text{Nb}_2\text{O}_9$ single-phase nanocrystallites synthesized via sucrose-assisted sol-gel combustion method. *J. Mater. Sci.* 53 (16), 11584–11594.
- Almashhori, K., Ali, T.T., Saeed, A., Alwafi, R., Aly, M., Al-Hazmi, F.E., 2020. Antibacterial and photocatalytic activities of controllable (anatase/rutile) mixed phase TiO_2 nanophotocatalysts synthesized via a microwave-assisted sol-gel method. *New J. Chem.* 44 (2), 562–570.
- Al-Muntaser, A., Abdelghany, A., Abdelrazek, E., Elshahawy, A., 2020. Enhancement of optical and electrical properties of PVC/PMMA blend films doped with $\text{Li}_4\text{Ti}_5\text{O}_{12}$ nanoparticles. *J. Mater. Res. Technol.* 9 (1), 789–797.
- Al-Muntaser, A.A., Pashameah, R.A., Sharma, K., Alzahrani, E., Tarabiah, A.E., 2022a. Reinforcement of structural, optical, electrical, and dielectric characteristics of CMC/PVA based on GNP/ZnO hybrid nanofiller: Nanocomposites materials for energy-storage applications. *Int. J. Energy Res.* n/a (n/a).
- Al-Muntaser, A., Pashameah, R.A., Sharma, K., Alzahrani, E., Farea, M., Morsi, M., 2022b. $\alpha\text{-MoO}_3$ nanobelts/CMC-PVA nanocomposites: hybrid materials for optoelectronic and dielectric applications. *J. Polym. Res.* 29 (7), 1–11.
- Al-Muntaser, A.A., Pashameah, R.A., Sharma, K., Alzahrani, E., Tarabiah, A.E., 2022c. Reinforcement of structural, optical, electrical, and dielectric characteristics of CMC/PVA based on GNP/ZnO hybrid nanofiller: Nanocomposites materials for energy-storage applications. *Int. J. Energy Res.*
- Al-Muntaser, A.A., Pashameah, R.A., Saeed, A., Alwafi, R., Alzahrani, E., AlSubhi, S.A., Yassin, A.Y., 2023. Boosting the optical, structural, electrical, and dielectric properties of polystyrene using a hybrid GNP/Cu nanofiller: novel nanocomposites for energy storage applications. *J. Mater. Sci.-Mater. Electron.* 34 (7), 678.
- Al-Muntaser, A.A., Pashameah, R.A., Tarabiah, A.E., Alzahrani, E., AlSubhi, S.A., Saeed, A., Al-Harhi, A.M., Alwafi, R., Morsi, M.

- A., 2023. Structural, morphological, optical, electrical and dielectric features based on nanoceramic Li₄Ti₅O₁₂ filler reinforced PEO/PVP blend for optoelectronic and energy storage devices. *Ceram. Int.*
- Berestennikov, A.S., Aleshin, A.N., 2017. Mechanisms of charge transport and resistive switching in composite films of semiconducting polymers with nanoparticles of graphene and graphene oxide. *J. Phys. Conf. Ser.* 917, (9) 092019.
- Bet-Moushoul, E., Mansourpanah, Y., Farhadi, K., Tabatabaei, M., 2016. TiO₂ nanocomposite based polymeric membranes: a review on performance improvement for various applications in chemical engineering processes. *Chem. Eng. J.* 283, 29–46.
- Chelouche, A., Touam, T., Djouadi, D., Aksas, A., 2014. Synthesis and characterizations of new morphological ZnO and Ce-doped ZnO powders by sol–gel process. *Optik* 125 (19), 5626–5629.
- Cho, K.S., Hong, J.-I., Chung, C.I., 2004. Effects of ZnO nanoparticles on thermal stabilization of polymers. *Polym. Eng. Sci.* 44 (9), 1702–1706.
- Choudhary, S., 2018. Structural, optical, dielectric and electrical properties of (PEO–PVP)–ZnO nanocomposites. *J. Phys. Chem. Solid* 121, 196–209.
- Choudhury, K.R., Samoc, M., Patra, A., Prasad, P.N., 2004. Charge carrier transport in poly (N-vinylcarbazole): CdS quantum dot hybrid nanocomposite. *J. Phys. Chem. B* 108 (5), 1556–1562.
- Coats, A.W., Redfern, J., 1964. Kinetic parameters from thermogravimetric data. *Nature* 201 (4914), 68–69.
- Croce, F., Appetecchi, G.B., Persi, L., Scrosati, B., 1998. Nanocomposite polymer electrolytes for lithium batteries. *Nature* 394 (6692), 456–458.
- Cui, K.M., Tria, M.C., Pernites, R., Binag, C.A., Advincula, R.C., 2011. PVK/MWNT electrodeposited conjugated polymer network nanocomposite films. *ACS Appl. Mater. Interfaces* 3 (7), 2300–2308.
- Das, D., Gopikrishna, P., Narasimhan, R., Singh, A., Dey, A., Iyer, P. K., 2016. White polymer light emitting diodes based on PVK: the effect of the electron injection barrier on transport properties, electroluminescence and controlling the electroplex formation. *Phys. Chem. Chem. Phys.* 18 (48), 33077–33084.
- Das, S., Jana, B., Debnath, T., Ghoshal, A., Das, A.K., Patra, A., 2017. Strategy toward designing semiconducting polymer nanoparticle–multichromophoric dye assembly. *J. Phys. Chem. C* 121 (7), 4050–4059.
- Dhatarwal, P., Sengwa, R.J., Choudhary, S., 2018. Effectively improved ionic conductivity of montmorillonite clay nanoplatelets incorporated nanocomposite solid polymer electrolytes for lithium ion-conducting devices. *SN Appl. Sci.* 1 (1), 112.
- Dimapilis, E.A.S., Hsu, C.-S., Mendoza, R.M.O., Lu, M.-C., 2018. Zinc oxide nanoparticles for water disinfection. *Sustainable Environ. Res.* 28 (2), 47–56.
- El Gohary, H.G., Alhagri, I.A., Qahtan, T.F., Al-Hakimi, A.N., Saeed, A., Abolaban, F., Alshammari, E.M., Asnag, G.M., 2023. Reinforcement of structural, thermal and electrical properties and antibacterial activity of PVA/SA blend filled with hybrid nanoparticles (Ag and TiO₂ NPs): Nanodielectric for energy storage and food packaging industries. *Ceram. Int.* 49 (12), 20174–20184.
- El Miri, N., El Achaby, M., Fihri, A., Larzek, M., Zahouily, M., Abdelouahdi, K., Barakat, A., Solhy, A., 2016. Synergistic effect of cellulose nanocrystals/graphene oxide nanosheets as functional hybrid nanofiller for enhancing properties of PVA nanocomposites. *J. Carbohydrate Polym.* 137, 239–248.
- Elashmawi, I., Al-Muntaser, A., 2021. Influence of Co₃O₄ nanoparticles on the optical, and electrical properties of CMC/PAM polymer: combined FTIR/DFT study. *J. Inorg. Organometall. Polym. Mater.* 31 (6), 2682–2690.
- El-Gamal, S., Elsayed, M., 2020. Synthesis, structural, thermal, mechanical, and nano-scale free volume properties of novel PbO/PVC/PMMA nanocomposites. *Polymer* 206, 122911.
- El-Kader, F.A., Hakeem, N., Elashmawi, I., Ismail, A., 2013. Structural, optical and thermal characterization of ZnO nanoparticles doped in PEO/PVA blend films. *Aust. J. Basic Appl. Sci* 7 (10), 608–619.
- Fahimi, Z., Moradlou, O., 2020. Fabrication of ZnO@C foam: A flexible free-standing electrode for energy storage devices. *Mater. Des.* 189, 108525.
- Hermans, P.H., Weidinger, A., 1949. X-ray studies on the crystallinity of cellulose. *J. Polym. Sci.* 4 (2), 135–144.
- Hezma, A., Rajeh, A., Mannaa, M.A., 2019. An insight into the effect of zinc oxide nanoparticles on the structural, thermal, mechanical properties and antimicrobial activity of Cs/PVA composite. *Colloids Surf. A Physicochem. Eng. Asp.* 581, 123821.
- Hodge, R., Edward, G.H., Simon, G.P., 1996. Water absorption and states of water in semicrystalline poly (vinyl alcohol) films. *Polymer* 37 (8), 1371–1376.
- Jakić, M., Vrandečić, N.S., Klarić, I., 2013. Thermal degradation of poly (vinyl chloride)/poly (ethylene oxide) blends: Thermogravimetric analysis. *Polym. Degrad. Stab.* 98 (9), 1738–1743.
- Jiménez-Rosado, M., Gomez-Zavaglia, A., Guerrero, A., Romero, A., 2022. Green synthesis of ZnO nanoparticles using polyphenol extracts from pepper waste (*Capsicum annum*). *J. Clean. Prod.* 350, 131541.
- Kaur, J., Sharma, J.P., Singh, N., Pathak, D., Guleria, N., Singh, P.K., Sharma, P.K., 2022. Improvement in optical absorption and emission characteristics of polymethyl methacrylate in solution cast polymethyl methacrylate/polyvinyl carbazole polyblends. *J. Thermoplast. Compos. Mater.* 08927057221115714
- Kim, M., 2018. Brilliant photo-emission of crystalline hexagonal column of Alq. *Materials*.
- Koops, C., 1951. On the dispersion of resistivity and dielectric constant of some semiconductors at audiofrequencies. *J. Phys. Rev.* 83 (1), 121.
- Krylov, P.S., Berestennikov, A.S., Fefelov, S.A., Komolov, A.S., Aleshin, A.N., 2016. S-shaped current–voltage characteristics of polymer composite films containing graphene and graphene oxide particles. *Phys. Solid State* 58 (12), 2567–2573.
- Kubacka, A., Cerrada, M.L., Serrano, C., Fernández-García, M., Ferrer, M., Fernández-García, M., 2009. Plasmonic nanoparticle/polymer nanocomposites with enhanced photocatalytic antimicrobial properties. *J. Phys. Chem. C* 113 (21), 9182–9190.
- Kurniawan, R., Sutjahja, I.M., Winata, T., Herg, T.S., Ding, J., Rusydi, A., Darma, Y., 2017. Polarization behavior of zinc oxide thin films studied by temperature dependent spectroscopic ellipsometry. *Opt. Mater. Express* 7 (11), 3902–3908.
- Lai, Y.-S., Tu, C.-H., Kwong, D.-L., Chen, J.-S., 2005. Bistable resistance switching of poly (N-vinylcarbazole) films for nonvolatile memory applications. *J. Appl. Phys. Lett.* 87, (12) 122101.
- Langar, A., Sdiri, N., Elhouichet, H., Ferid, M., 2017. Structure and electrical characterization of ZnO-Ag phosphate glasses. *Results Phys.* 7, 1022–1029.
- Liu, S., Xiu, S., Shen, B., Zhai, J., Kong, L.B., 2016. Dielectric properties and energy storage densities of poly(vinylidene fluoride) nanocomposite with surface hydroxylated cube shaped Ba(0.6)Sr(0.4)TiO₃ nanoparticles. *Polymers (Basel)* 8 (2), 45.
- Malimabe, M.A., Dejene, B.F., Swart, H.C., Motlounge, S.V., Motaung, T.E., Kooa, L.F., 2020. Characterization of the incorporated ZnO doped and co-doped with Ce³⁺ and Eu³⁺ nanophosphor powders into PVC polymer matrix. *J. Mol. Struct.* 1202, 127339.
- Menazea, A., Elashmawi, I., Abd El-kader, F., Hakeem, N., 2018. Nanosecond pulsed laser ablation in liquids as new route for preparing polyvinyl carbazole/silver nanoparticles composite: spectroscopic and thermal studies. *J. Inorg. Organomet. Polym. Mater.* 28, 2564–2571.
- Menazea, A., Ismail, A., Elashmawi, I., 2020. The role of Li₄Ti₅O₁₂ nanoparticles on enhancement the performance of PVDF/PVK

- blend for lithium-ion batteries. *J. Mater. Res. Technol.-JMRT* 9 (3), 5689–5698.
- Michael, M.S., Prabakaran, S.R.S., 2004. Rechargeable lithium battery employing a new ambient temperature hybrid polymer electrolyte based on PVK + PVdF-HFP (copolymer). *J. Power Sources* 136 (2), 408–415.
- Miliute-Plepiene, J., Fr ane, A., Almasi, A.M., 2021. Overview of polyvinyl chloride (PVC) waste management practices in the Nordic countries. *Clean. Eng. Technol.* 4, 100246.
- Misra, S., Han, Y., 2020. Chapter 13 - Characterization of subsurface hydrocarbon/water saturation using Markov-chain Monte Carlo stochastic inversion of broadband electromagnetic logs. In: Misra, S., Li, H., He, J. (Eds.), *Machine Learning for Subsurface Characterization*. Gulf Professional Publishing, pp. 369–402.
- Moisan, J.-Y., Andr e, B., Lever, R., 1991. Xerographic dark discharge of PVK:TNF photoconductive material. *Chem. Phys.* 153 (1), 305–312.
- Morsi, M.A., Abdelrazek, E.M., Ramadan, R.M., Elashmawi, I.S., Rajeh, A., 2022. Structural, optical, mechanical, and dielectric properties studies of carboxymethyl cellulose/polyacrylamide/lithium titanate nanocomposites films as an application in energy storage devices. *Polym. Test.* 114, 107705.
- Morsi, M., Pashameah, R.A., Sharma, K., Alzahrani, E., Farea, M., Al-Muntaser, A., 2022. Hybrid MWCNTs/Ag nanofiller reinforced PVP/CMC blend-based polymer nanocomposites for multifunctional optoelectronic and nanodielectric applications. *J. Polym. Environ.*, 1–13.
- Nair, M.R., Thomas, G.V., Nair, M.G., 2007. Thermogravimetric analysis of PVC/ELNR blends. *Polym. Degrad. Stab.* 92 (2), 189–196.
- Nikam, P.N., Deshpande, V.D., 2018. Dielectric behavior of plasticized PVC/alumina nanocomposites influenced with DC biasing field. *Mater. Today: Proc.* 5 (1), 2254–2262.
- O'Rourke, M.B., Town, S.E.L., Dalla, P.V., Bicknell, F., Koh Belic, N., Violi, J.P., Steele, J.R., Padula, M.P., 2019. What is Normalization? The strategies employed in top-down and bottom-up proteome analysis workflows. *Proteomes*, 29.
- Onkar, S.G., Nagdeote, S.B., Wadatar, A.S., Kharat, P.B., 2020. Gas sensing behavior of ZnO thick film sensor towards H₂S, NH₃, LPG and CO₂. *J. Phys. Conf. Ser.* 1644, (1) 012060.
- Pleša, I., Nojinger, P.V., Schl ogl, S., Sumereder, C., Muhr, M., 2016. Properties of polymer composites used in high-voltage applications. *Polymers* 8 (5), 173.
- Ramesh, S., Liew, C.-W.-J.-M., 2013. Dielectric and FTIR studies on blending of [xPMMA-(1-x) PVC] with LiTFSI. *J. Measurement* 46 (5), 1650–1656.
- Ranjan, N., Kumar, R., Singh, R., Kumar, V., 2021. On polyvinyl chloride-polypropylene composite matrix for 4D applications: Flowability, mechanical, thermal and morphological characterizations. *J. Thermoplast. Compos. Mater.* 08927057211059754.
- Rehman, W.U., Khattak, M.T.N., Saeed, A., Shaheen, K., Shah, Z., Hussain, S., Bakhsh, E.M., Alraddadi, H.M., Fagieh, T.M., Akhtar, K., Khan, S.B., Khan, S.A., 2023. Co₃O₄/NiO nanocomposite as a thermocatalytic and photocatalytic material for the degradation of malachite green dye. *J. Mater. Sci.-Mater. Electron.* 34 (1), 15.
- Saeed, A., Al-Buriah, M.S., Razvi, M.A.N., Salah, N., Al-Hazmi, F. E., 2021. Electrical and dielectric properties of meridional and facial Alq₃ nanorods powders. *J. Mater. Sci.-Mater. Electron.* 32 (2), 2075–2087.
- Saeed, A., Adewuyi, S.O., Ahmed, H.A.M., Alharbi, S.R., Al Garni, S. E., Abolaban, F., 2022. Electrical and dielectric properties of the natural calcite and quartz. *SILICON* 14 (10), 5265–5276.
- Saeed, A., Abolaban, F., Al-Mhyawi, S.R., Albaidani, K., Al Garni, S. E., Al-Marhaby, F.A., Alwafi, R., Djouider, F., Qahtan, T.F., Asnag, 2023. Improving the polyethylene oxide/carboxymethyl cellulose blend's optical and electrical/dielectric performance by incorporating gold quantum dots and copper nanoparticles: nanocomposites for energy storage applications. *J. Mater. Res. Technol.-JMRT* 24, 8241–8251.
- Santos, C.M., Mangadla, J., Ahmed, F., Leon, A., Advincula, R.C., Rodrigues, D.F., 2012. Graphene nanocomposite for biomedical applications: fabrication, antimicrobial and cytotoxic investigations. *Nanotechnology* 23, (39) 395101.
- Sasani Ghamsari, M., Alamdari, S., Han, W., Park, H.H., 2017. Impact of nanostructured thin ZnO film in ultraviolet protection. *Int. J. Nanomed.* 12, 207–216.
- Soliman, T.S., Rashad, A.M., Ali, I.A., Khater, S.I., Elkalashy, S.I., 2020. Investigation of linear optical parameters and dielectric properties of polyvinyl alcohol/ZnO nanocomposite films. *Phys. Status Solidi (a)* 217 (19), 2000321.
- Sonone, R., Raut, V., Murhekar, G., 2014. Structural and electroluminescence properties of pure PVK and doped TiO₂ polymer thin films. *J. Adv. Res. Chem. Sci.* 1 (1), 87–94.
- Sudeepan, J., Kumar, K., Barman, T.K., Sahoo, P., 2014. Study of friction and wear of ABS/ZnO polymer composite using Taguchi technique. *Procedia Mater. Sci.* 6, 391–400.
- Taha, T., 2017. Optical and thermogravimetric analysis of Pb₃O₄/PVC nanocomposites. *J. Mater. Sci. Mater. Electron.* 28, 12108–12114.
- Taha, T., Hendawy, N., El-Rabaie, S., Esmat, A., El-Mansy, M., 2019. Effect of NiO NPs doping on the structure and optical properties of PVC polymer films. *Polym. Bull.* 76, 4769–4784.
- Tarabiah, A., Alhadlaq, H.A., Alaizeri, Z.M., Ahmed, A.A., Asnag, G., Ahamed, M., 2022. Enhanced structural, optical, electrical properties and antibacterial activity of PEO/CMC doped ZnO nanorods for energy storage and food packaging applications. *J. Polym. Res.* 29 (5), 1–16.
- Thinh, P.X., Basavaraja, C., Kim, D., Huh, D.S., 2012. Characterization and electrochemical behaviors of honeycomb-patterned poly (N-vinylcarbazole)/polystyrene composite films. *Polym. Bull.* 69 (1), 81–94.
- Wang, Z., Bockstaller, M.R., Matyjaszewski, K., 2021. Synthesis and applications of ZnO/polymer nanohybrids. *ACS Mater. Lett.* 3 (5), 599–621.
- Wang, S., Yang, S., Yang, C., Li, Z., Wang, J., Ge, W., 2000. Poly (N-vinylcarbazole)(PVK) photoconductivity enhancement induced by doping with CdS nanocrystals through chemical hybridization. *J. Phys. Chem. B* 104 (50), 11853–11858.
- Willander, M., Nur, O., Sadaf, J.R., Qadir, M.I., Zaman, S., Zainelabdin, A., Bano, N., Hussain, I., 2010. Luminescence from zinc oxide nanostructures and polymers and their hybrid devices. *Materials*, 2643–2667.
- Willander, M., Nur, O., Zaman, S., Zainelabdin, A., Bano, N., Hussain, I., 2011. Zinc oxide nanorods/polymer hybrid heterojunctions for white light emitting diodes. *J. Phys. D: Appl. Phys.* 44, (22) 224017.
- Yang, C.-C., Yang, J.M., Wu, C.-Y., 2009. Poly(vinyl alcohol)/poly (vinyl chloride) composite polymer membranes for secondary zinc electrodes. *J. Power Sources* 191 (2), 669–677.
- Yu, S., Hing, P., Hu, X., 2000. Dielectric properties of polystyrene-aluminum-nitride composites. *J. Appl. Phys.* 88 (1), 398–404.
- Zhang, T., Nazarov, R., Pham, L.Q., Soboleva, V., Demchenko, P., Uspenskaya, M., Olekhovich, R., Khodzitsky, M., 2020. Polymer composites based on polyvinyl chloride nanofibers and polypropylene films for terahertz photonics. *Opt. Mater. Express* 10 (10), 2456–2469.
- Zhang, L., Yin, L., Wang, C., Lun, N., Qi, Y., 2010. Sol-gel growth of hexagonal faceted ZnO prism quantum dots with polar surfaces for enhanced photocatalytic activity. *ACS Appl. Mater. Interfaces* 2 (6), 1769–1773.